Functional Polyoxometalate Thin Films via Electrostatic Layer-by-Layer Self-Assembly*

Shaoqin Liu,[1] Dirk Volkmer,[2] and Dirk G. Kurth[1, 3]

INTRODUCTION

Polyoxometalates (POMs) are well-defined, discrete transition metal oxide clusters with a large range of possible applications in fundamental and applied science including catalysis [1], electrochemistry [2], electrooptics [3], medicine [4], corrosion protection, dyes and pigments, dopants in (non-)conductive polymers and sol-gels, bleaching of paper pulp, as well as analytical chemistry [5]. In contrast to many semiconductor nanoparticles

---

* Dedicated to Professor Achim Müller on the occasion of his 65th anniversary.

[1] Max Planck Institute of Colloids and Interfaces, D-14424 Potsdam, Germany.

[2] University of Bielefeld, Faculty of Chemistry, AC1, D-33501 Bielefeld, Germany. E-mail: dirk.volkmer@uni-bielefeld.de

[3] To whom correspondence should be addressed. E-mail: kurth@mpikg-golm.mpg.de

and quantum dots, POMs are strictly uniform at the atomic level. A bewildering variety of POM structures has been characterized since 1933, when the seminal X-ray crystal structure analysis of the Keggin anion, $[PW_{12}O_{40}]^{3-}$, appeared in the literature [6]. This work has recently culminated in the discovery of giant nanosized polymolybdate clusters [7], mainly by the work of Achim Muller *et al.* to whom this special issue is dedicated.

Apart from their aesthetically pleasant structures, a particularly attractive feature is the ability of the POM metal-oxygen framework to undergo rapid multiple reversible reductions, which is often accompanied by coloration [8]. If the addenda ions are all identical, the electrons can be delocalized on the POM framework through rapid electron hopping (*intermolecular electron transfer*). The reduced POMs are active electrocatalysts for the hydrogen evolution reaction and oxygen reduction [9]. The property of POMs to exhibit different colors in their oxidized and reduced states is perhaps the most promising effect for the fabrication of electrochromic coatings, which can be employed in various applications, such as smart windows for the modulation of incoming light and in flat-panel display devices. The extinction coefficient of the photo-reduced mixed-valent POM is comparable to that of organic dyes, however, the long-term photochemical stability of POMs is far *superior* to that of organic molecules. Photochromic properties arise in the presence of certain counter ions, such as alkylammonium, anilinium and pyridinium, which can undergo photoinduced proton transfer to the POM framework. The reduction of the POM cluster results in accumulation of negative charge, which increases the basicity of the POM anion. The reduction process may, therefore, be accompanied by concomitant protonation and, as a result, the redox properties of POMs are markedly pH sensitive [9].

The exploitation of *value-adding* properties of POMs in advanced materials has remained elusive until recently, mainly due to the fact that these compounds are commonly obtained as crystalline solids that are hard to process. Recent studies show, however, that giant, spherical POM systems, including some wheel-shaped and hollow "*Keplerate*" molecules, spontaneously form "*necklaces*" and 2D layers by a solid state reaction and slowly self-assemble into a vesicle structure in polar solvents [10]. In order to support, handle, manipulate, and operate devices that contain POMs as functional components, it will be advantageous to arrange the clusters in surface-confined structures, however, until recently there have been no generic methodologies available to achieve this goal [11].

In recent years different strategies have been devised to solve this problem. For instance, we have explored methods to tailor the surface chemical properties of POMs as a means to engineer novel nano- and

mesoscopic supramolecular architectures. Here, we rely on self-assembly of POMs and suitable surfactants. In these so-called *surfactant-encapsulated clusters* (SECs) a single POM cluster resides within a hydrophobic shell of surfactant molecules, leading to a discrete, nearly spherical assembly [12]. SECs are attractive modules for molecular devices because they combine the physicochemical properties of the inorganic polyoxometalate core with the diverse assets of surface-active organic compounds including wetting, adhesion, solubility as well as bio-compatibility. The latest development in this field is the design of artificial enzymes, so-called *dendrizymes*, which mimic the structure and function of naturally occurring catalytically active metalloproteins [13].

A very versatile technique, known as electrostatic layer-by-layer self-assembly (ELSA) [14], has been explored to form well-defined layered architectures of POMs. Layer formation is based on the rather unspecific electrostatic attraction between the negatively charged POMs and positively charged moieties, including transition metal complexes, cationic surfactants, polycations, and bipolar pyridine. This technique provides extensive control of structure, order, and functionality. The current status of development in this particular field will be highlighted in the present review with an emphasis on some of the most promising applications in various fields of materials science.

THE FORMATION OF ULTRA THIN MULTILAYERS

Self-assembly of alternating layers of POM anions and oppositely charged species is deceptively simple. The ELSA approach is schematically summarized in Fig. 1. For example, starting with a negatively charged substrate, such as a layer of polystyrene-sulfonate (PSS) or a charged monolayer of an alkyl-silane [15] or alkyl-thiol [16], its immersion into a polycation solution leads to the adsorption of the polycations, thereby recharging the surface. Typically, a few minutes are sufficient to establish a complete layer [17]. After rinsing the sample, immersion into a POM solution results in adsorption of the next layer. Repetition of this alternating deposition leads to build-up of the multilayer. The only requirement is that the components are sufficiently charged in order to adsorb irreversibly at the interface.

Several POMs of different shape, size, and charge were successfully incorporated in multilayers (Fig. 2) [18–25]. Table I summarizes some of the cations/POM combinations used to date. In addition to random coil like polycations other cationic motives have also been tailed into multilayers. These include transition metal complexes, cationic surfactants [19], dendrimers [26], dicationic amphiphiles [25], and bipolar pyridines [19].

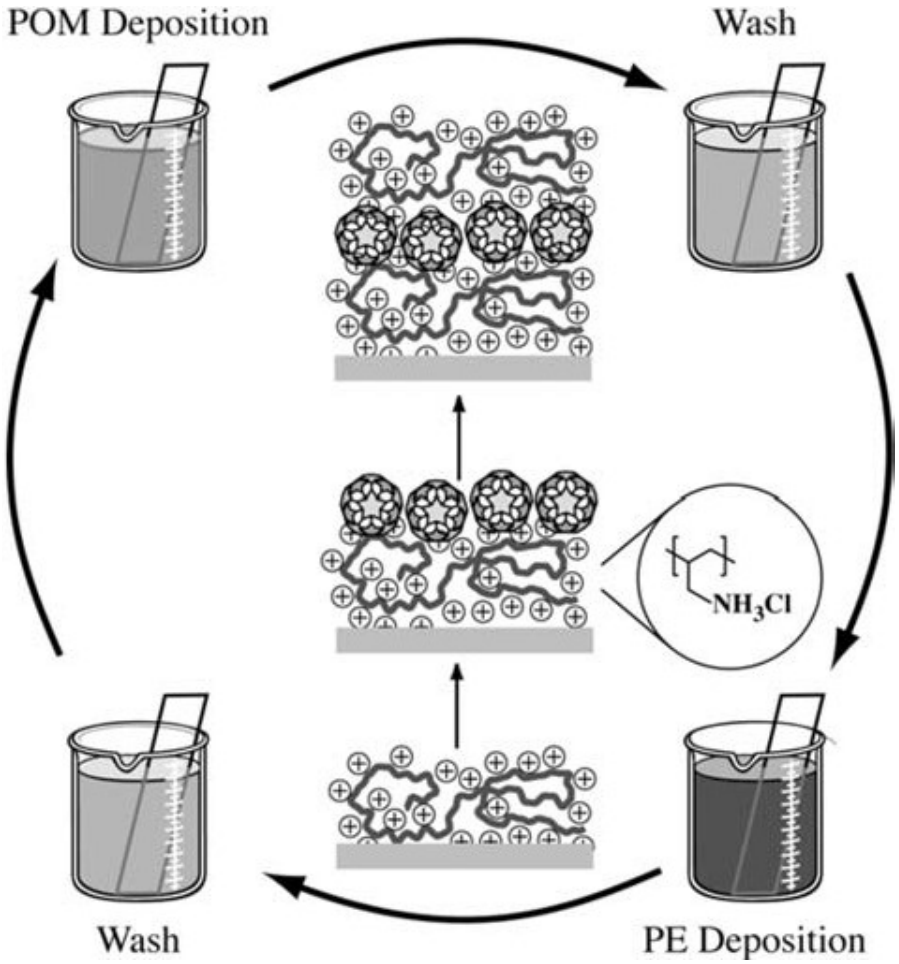

Fig. 1. ELSA relies primarily on electrostatic interactions of oppositely charged adsorbates. Multilayer growth proceeds in a sequential process, in which the substrate is immersed in dilute solutions of oppositely charged species and intermittent washing steps. Combinations of different components in a single film are easily put into practice.

Here, the surface coverage is reported in number of monolayers with respect to the packing density of the corresponding POM in the crystalline solid. For all POM-based multilayers, as with many other systems prepared by this technique, the total thickness of multilayer assemblies increases linearly with the number of adsorbed layers, indicating a stepwise and regular growth process. The final coverage does not depend on the dipping time, it, however, depends on the experimental parameters, such as ionic strength. The occurrence of regular growth is consistent with a build-up of an excess interfacial charge by the POM anions, which the next layer of positively charged PE can bind to.

The deposition process is governed by a delicate balance of adsorption and desorption equilibria. While the immersion step should lead to the irreversible adsorption of a controlled amount of material onto the interface, the rinsing process is used for desorption of excess, loosely bound species. The optimization of ELSA in terms of controlling the deposited amount in these two competing processes requires the judicious selection of

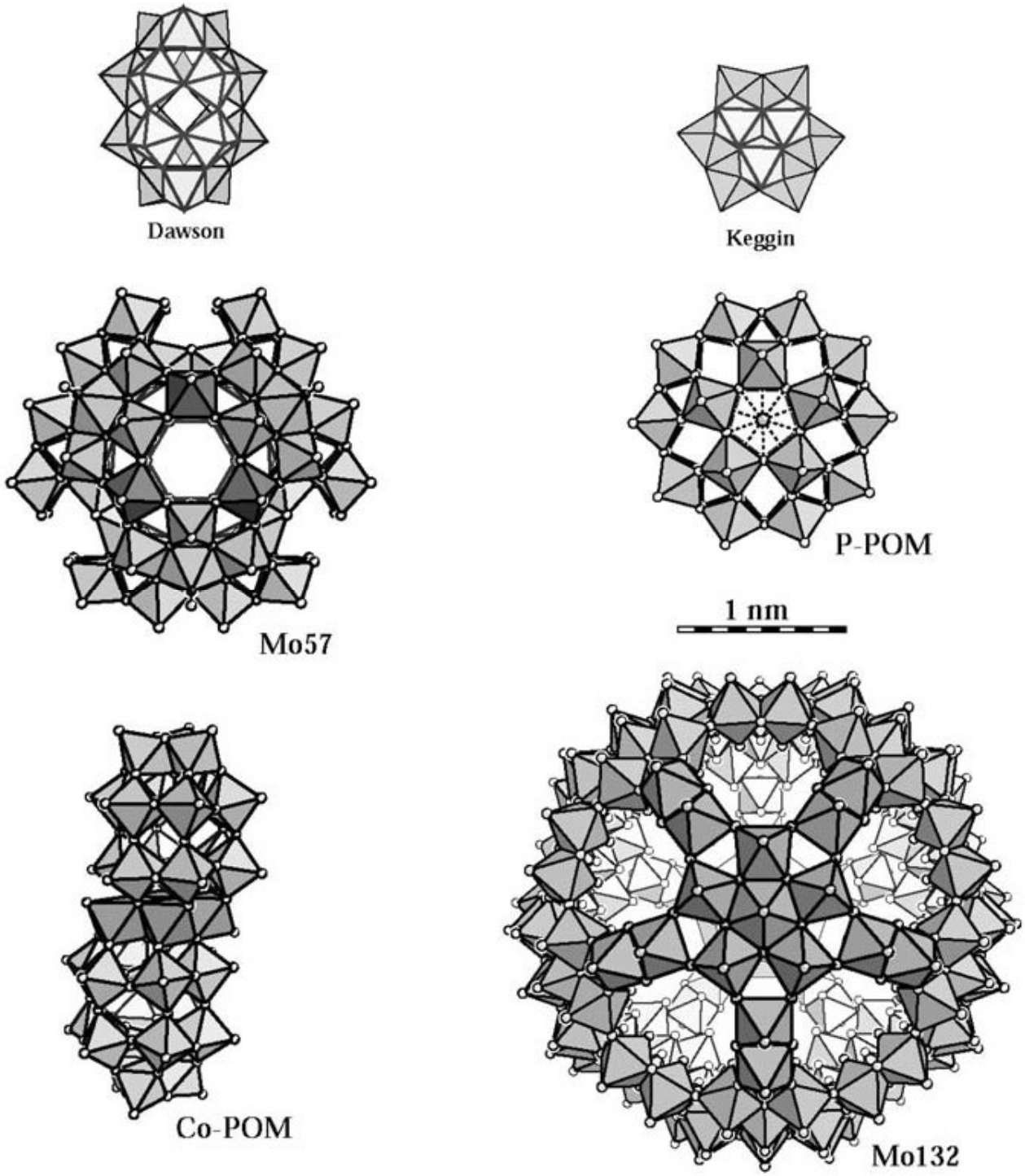

Fig. 2. Structures of some of the POMs used for the fabrication of ELSA multilayers. **Keggin**: $[XM_{12}O_{40}]^{3-/4-}$ (X = P, Si, M = W, Mo). **Dawson**: $[P_2M_{18}O_{62}]^{6-}$ (M = W, Mo). **Preyssler (P-POM)**: $[M(H_2O)P_5W_{30}O_{110}]^{14/12-}$ (M = Na, Eu). The **P-POM** has the shape of a flattened ellipsoid with dimensions 1.3×1.7 nm. **Co-POM**: $[Co^{II}_4(H_2O)_2P_4W_{30}O_{112}]^{16-}$. The "sandwich" type Co(II)-substituted **Co-POM** is approx. 2.3 nm in length and 1.4 nm in width. **Mo57**: $[H_3Mo_{57}V_6(NO)_6O_{183}(H_2O)_{18}]^{21-}$. The external form of **Mo57** is similar to **P-POM** with dimensions of 1.6×2.4 nm. **Mo132**: Giant Keplerate $[Mo_{132}O_{372}(CH_3COO)_{30}(H_2O)_{72}]^{42-}$. The nearly spherical **Mo132** with a diameter of approx. 3 nm shows promising perspectives in host-guest chemistry and size-selective catalysis because it possesses an open Mo–O framework architecture that encloses a central cavity with an approximate inner diameter of 1.7 nm. The **Mo132** framework spans (Mo–O) 9-ring openings with an average ring aperture of 0.43 nm, which is comparable in size to pores in zeolitic architectures.

Table I. ELSA Multilayers of POMs

POM compound	Cationic layer	Surface coverage[a]	Ref.
$[W_{10}O_{32}]^{4-}$	PDDA	2 ~ 3	[19a]
$[Mo_8O_{26}]^{4-}$	PEI, PAH	2 ~ 3	[19b]
$[PW_{12}O_{40}]^{3-}$	CTA, DTA, $PVPH^+$, $Ru(bpy)_3^{2+}$, DADD $Fe(phen)_3^{2+}$, CuPEI,		
$[SiW_{12}O_{40}]^{4-}$	CTA, DTA, $PVPH^+$	1 ~ 2	
$[SiMo_{11}VO_{40}]^{5-}$	$PVPH^+/Os(bpy)_3^{2+}$		
$[P_2Mo_{18}O_{62}]^{6-}$	CTA, CP, $PVPH^+$, $Ru(bpy)_3^{2+}$, DADD, $Os(bpy)_3^{2+}$		
$[P_2W_{18}O_{62}]^{6-}$	$Ru(bpy)_3^{2+}$, RuDen, $Os(bpy)_3^{2+}$		
$[Eu^{(III)}(H_2O)P_5W_{30}O_{110}]^{12-}$	PSS, PAH	0.5 ~ 3	[22a, 23]
$[Na(H_2O)P_5W_{30}O_{110}]^{14-}$	PSS, PAH	0.5 ~ 3	[22a]
$[Co_4^{II}(H_2O)_2P_4W_{30}O_{112}]^{16-}$	PSS, PAH	1 ~ 5	[22b]
$[H_3Mo_{57}V_6(NO)_6O_{183}(H_2O)_{18}]^{21-}$	PAH	~ 0.6	[21]
$[Mo_{132}O_{372}(CH_3COO)_{30}(H_2O)_{72}]^{42-}$	PAH	~ 0.5	[20]

[a] The surface coverage is based on the packing density in the crystalline solid.

pH and ionic strength of the dipping solutions as well as the careful control of the kinetics of the process. For instance, the layering of smaller POM anions is critically affected by the pH of the solutions. The presence of protons in the dipping solutions is known to significantly enhance the irreversibly adsorbed quantity of POM anions [19, 20].

For smaller POMs, the surface coverage can be adjusted from sub-monolayer to multilayer coverage simply by adjusting the ionic strength of the dipping solutions. This is demonstrated in Fig. 3 for the deposition of $[Eu^{(III)}(H_2O)P_5W_{30}O_{110}]^{12-}$ and PAH [22]. If no salt is added to the POM solution, residual electrostatic and dipolar repulsion within the interfacial layer keep the surface-confined POM anions separated, thereby resulting in sub-monolayer coverage, compared to the packing density of the POMs in the crystalline solid. In the presence of salt in the POM dipping solutions, the surface coverage increases to approx. a monolayer. The high ionic strength screens repulsive interactions, thus, the anions can move together more closely. It is interesting to note that at a very high ionic strength of the dipping solution, regular film growth may fail, which is in marked contrast to the adsorption of polyelectrolytes [26]. If, in addition, salt is added to the PAH dipping solution, the surface coverage increases to approx. two monolayers, which is attributed to penetration of POM anions into the top

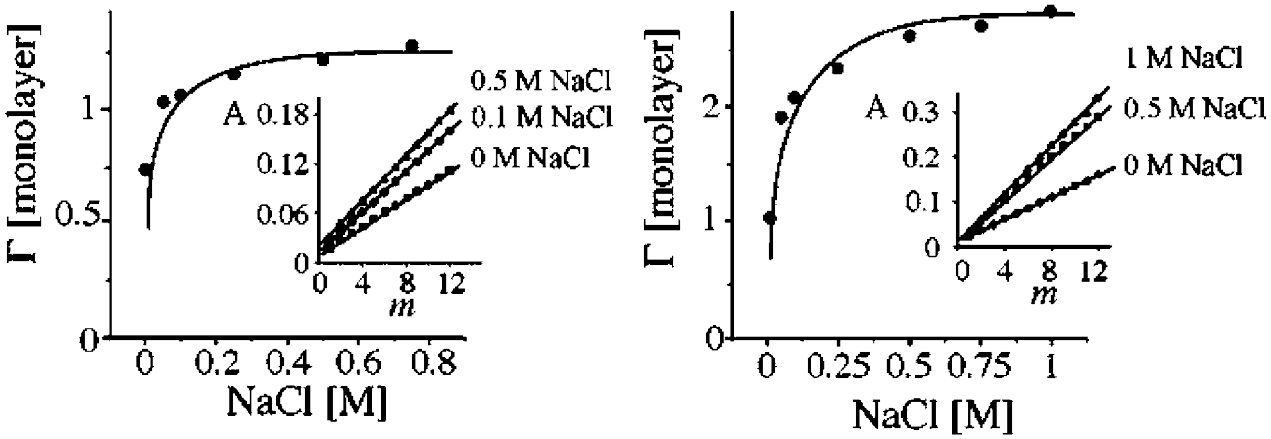

Fig. 3. The surface coverage per layer, Γ, of **Eu-POM** in (**Eu-POM**/PAH)$_m$ multilayers, as a function of NaCl concentration of the **Eu-POM** (left) and PAH solution (right). Left: PAH is deposited from aqueous solution containing no NaCl. Right: **Eu-POM** is deposited from aqueous solution containing 0.1 M NaCl. (Adapted from Ref. 22a.)

polyelectrolyte layer. However, the packing density of larger POM anions (**Mo132** and **Mo57**) does not depend so strongly on the ionic strength of the dipping solutions [20, 21]. In these cases, the packing density corresponds to sub-monolayer coverage. Most likely, the repulsive electrostatic and dipolar interactions are not compensated as efficiently in a two-dimensional film as for smaller POMs. Finally, the properties of the multilayers depend primarily on the choice of the building blocks used and their rational organization. In general, the use of large cationic surfactants has been found to increase the surface coverage during the alternate immersion, while macromolecular polycations are preferred for providing overall stability (prevention of decomposition and desorption upon repetitive cycling).

This method, therefore, provides control over film growth and thickness at the nanometer-scale. It does not require specialized equipment, or substrates, and it is readily adapted for automated fabrication. Furthermore, it is economical and readily amenable to scaling-up for the fabrication of large area, defect-free devices on any kind and shape of surfaces. The deposited films are mechanically robust and generally permeable for small molecules.

STRUCTURAL CHARACTERIZATION OF POM MULTILAYERS

UV-vis spectroscopy is probably the easiest way to monitor multilayer buildup, because of the strong characteristic adsorption band of POM anions in the range of 200–400 nm. Equivalent to measuring the optical absorbance, one can also determine the film thickness by ellipsometry or X-ray reflectometry as shown in Fig. 4. Further, X-ray reflectometry

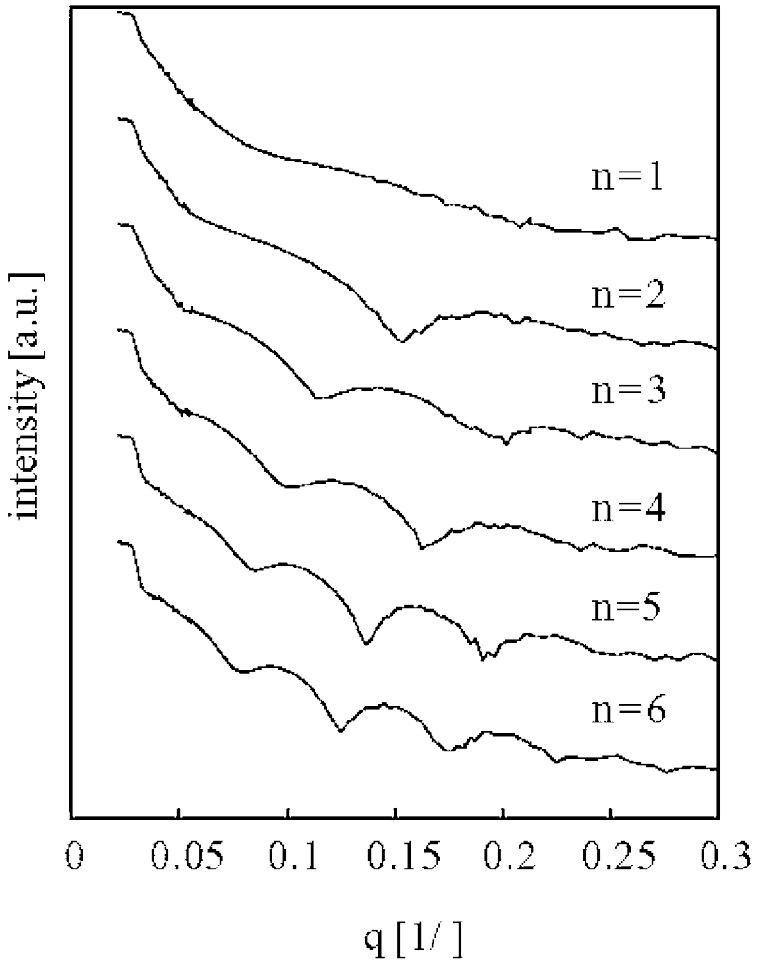

Fig. 4. X-ray reflectivity curves of alternating (**Mo132**/PAH)$_n$ multilayers on silicon. (Adapted from Ref. 21.)

provides evidence for the interior multilayer architecture and structural differences depending on the POM anion. Well-resolved Kiessig fringes occur in films of **Mo132**/PAH and **Mo57**/PAH [20, 21]. These multilayers are, therefore, homogenous at the macroscopic length scale. The total interfacial roughness is typically below 1 nm. No Bragg peaks are observed in these films indicating the lack of internal structure (stratification), which is attributed to the sub-monolayer coverage. However, in general, these multilayers are not strictly stratified because adjacent polyelectrolyte layers partially interpenetrate and are also less ordered than self-assembled monolayers or Langmuir–Blodgett (LB) films [27, 28]. However, for the smaller POMs, X-ray reflectometry does not resolve Kiessig fringes. Obviously, the interfacial roughness is too large to provide coherent interference of the X-rays from the top and bottom of the ELSA layer. The smaller POMs are probably more dispersed across the interface and penetrate the polyelectrolyte matrix more easily, therefore, reducing the degree of striation. However, Kiessig fringes become apparent if an additional PAH/PSS layer pair is placed on top of the multilayer. These complementary methods are simple to use and provide elementary

information on deposition and structure. Many other analytical tools are available to study adsorption kinetics, layer growth and structure. Most POM anions can undergo a rapid reversible reduction. Therefore, cyclic voltammetry (CV) is another frequently used tool in POM multilayer research [19, 20, 23, 24].

ELECTROCHROMIC DISPLAY DEVICES

In terms of possible components for electrochromic devices, POMs are promising candidates due to their ability to undergo a rapid reversible reduction accompanied by coloration. Very stable electrochromic coatings have been obtained by layering CTA with $[SiW_{12}O_{40}]^{4-}$, $Fe(phen)_3^{2+}$, and $[PW_{12}O_{40}]^{3-}$ [19a], $Os(bpy)_3^{2+}$ in combination with $[P_2Mo_{18}O_{62}]^{6-}$ [19b], and PDDA and $[W_{10}O_{32}]^{4-}$ [19a]; they could be cycled 60 to 400 times. A multicomponent electrochromic film has also been prepared by self-assembling protonated poly(4-vinylpyridine) with $[SiW_{12}O_{40}]^{4-}$ (inner film) and isopolymolybdate (outer film) to create a bistable switching system [19a].

To move towards realistic technological implementations, we selected the europium derivative of the Preyssler anion, $(NH_4)_{11.5}K_{0.5}[Eu(H_2O)P_5W_{30}O_{110}]\cdot 34H_2O$, (**Eu-POM**), as active component because it exhibits reversible electrochemical behavior accompanied by a large electrochromic response [29]. As can be seen in Fig. 5, the oxidized form of **Eu-POM** is completely transparent in the visible region, while the reduced **Eu-POM** exhibits a broad absorption band at approx. 700 nm. Each individual redox step is accompanied by an increasing coloration of the solution.

Device fabrication rests on principles of ELSA deposition of **Eu-POM**, PAH, and PSS on indium tin oxide (ITO) coated glass slides. A visually noticeable optical contrast (transparent to dark blue) during potential scanning manifests that the film is electrochromic. High optical contrast is readily achieved even for thin films. The UV/vis spectrum of the $(PSS/PAH/\textbf{Eu-POM}/PAH)_{20}$ modified ITO electrode shown in Fig. 5 is recorded during cyclic voltammetry. The absorbance at 700 nm, $A_{700\,nm}$, for a $(PSS/PAH/\textbf{Eu-POM}/PAH)_{20}$ modified ITO electrode increases to 0.12. For a $(PSS/PAH/\textbf{Eu-POM}/PAH)_{100}$ modified ITO electrode, $A_{700\,nm}$ becomes as large as 0.7. A single PSS/PAH/**Eu-POM**/PAH layer generates an optical density of 0.006 in the reduced state. A film less than 1 μm thick would create an optical density of approx. 1, which is sufficient for many practical device applications.

A representative time dependence of absorbance of a $(PSS/PAH/\textbf{Eu-POM}/PAH)_{20}$ multilayer at 700 nm during potential-step chronoamperometry is illustrated in Fig. 5 (right). Both current and absorbance

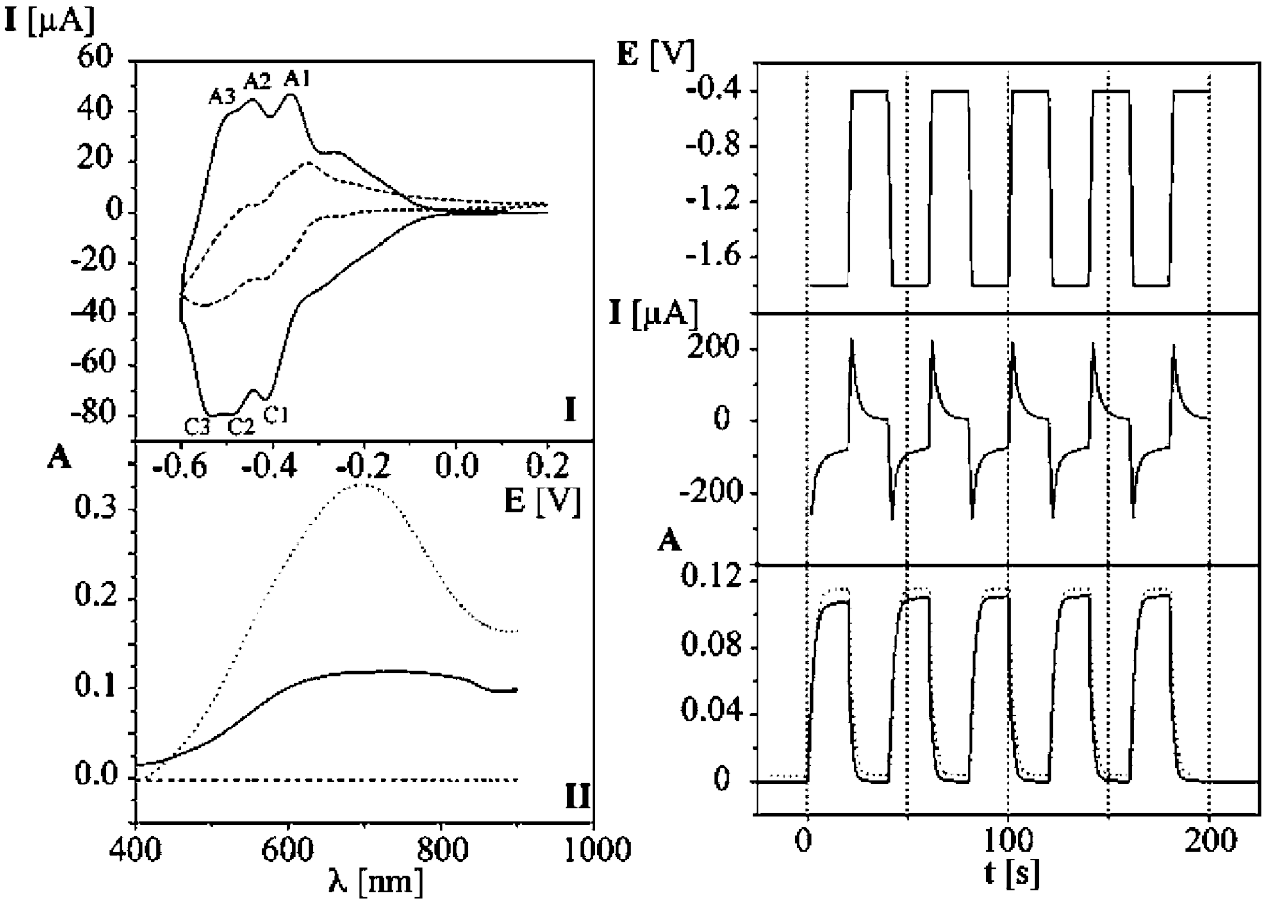

Fig. 5. Left: (I) CVs of **Eu-POM** in solution (dashed line, ITO electrode, 0.25 mM, ordinate magnified 5×) and a $(PSS/PAH/\textbf{Eu-POM}/PAH)_{20}$ multilayer (solid line, ITO electrode). (II) UV-vis spectra of oxidized (dashed line) and reduced (dotted line) **Eu-POM** in solution and a reduced $(PSS/PAH/\textbf{Eu-POM}/PAH)_{20}$ multilayer (solid line). Right: Potential, E, current, I, and absorbance, A, at 700 nm of the $(PSS/PAH/\textbf{Eu-POM}/PAH)_{20}$ coated ITO electrode to subsequent double potential steps between −0.4 and −1.8 V. Bottom: 1st cycle (solid line) and 500th (dashed line) cycle; traces are offset for clarity. The response time for coloration and bleaching is 4.2 and 4.4 s, respectively. (Adapted from Ref. 23a.)

respond within seconds during coloration and bleaching. The multilayer has good stability and reversibility as the CVs, the response times for coloration and bleaching, and the absorbance do not change noticeably even after 500 cycles. The multilayers also show a considerable optical memory that is, after reduction, the layer remains in the colored state even if the potential source is disconnected. Therefore, it is possible to display information with this device without power consumption. The low operation voltage and low power consumption are additional advantages of the device. Power is required only for switching and leakage currents can be minimized by operating the device under open circuit conditions. The method is readily extended to patterned substrates, so films can be prepared on predefined areas. Moreover, the devices can be prepared under ambient conditions by a robot.

SENSING APPLICATION OF THE MULTILAYER ASSEMBLIES

A large number of POMs undergo a series of reversible one- and two-electron reductions, which facilitates their use as redox catalysts. By selecting suitable cationic motives, the POM-based multilayer can be explored as a two-component, bifunctional electrocatalyst that can catalyze both reduction and oxidation. Cox *et al.* immobilized the ruthenium metallodendrimer (RuDen) on the electrode-adsorbed Dawson-type POM anion, $[P_2W_{18}O_{62}]^{6-}$ [26]. The obtained electrodes are highly organized, bifunctional catalytical systems, which are electrocatalytically active toward reduction of iodate and oxidation of arsenite (as shown in Fig. 6).

The reduction of POM increases the negative charge density of the metal-oxide framework and thus their basicity. As a consequence, the reduction is generally pH-dependent. This feature provides an opportunity to use POMs as electrochemical probes to survey microenvironmental effects. We selected **Co-POM** because of its good pH stability (pH $2 \sim 9$). It is interesting to note that the details of the electrochemical response of **Co-POM**-containing multilayers depend on the layer architecture. The CVs of (PSS/PAH/**Co-POM**/PAH)$_{10}$ and (**Co-POM**/PAH)$_{10}$ modified electrodes are shown in Fig. 7. The (PSS/PAH/Co-POM/PAH)$_{10}$ modified

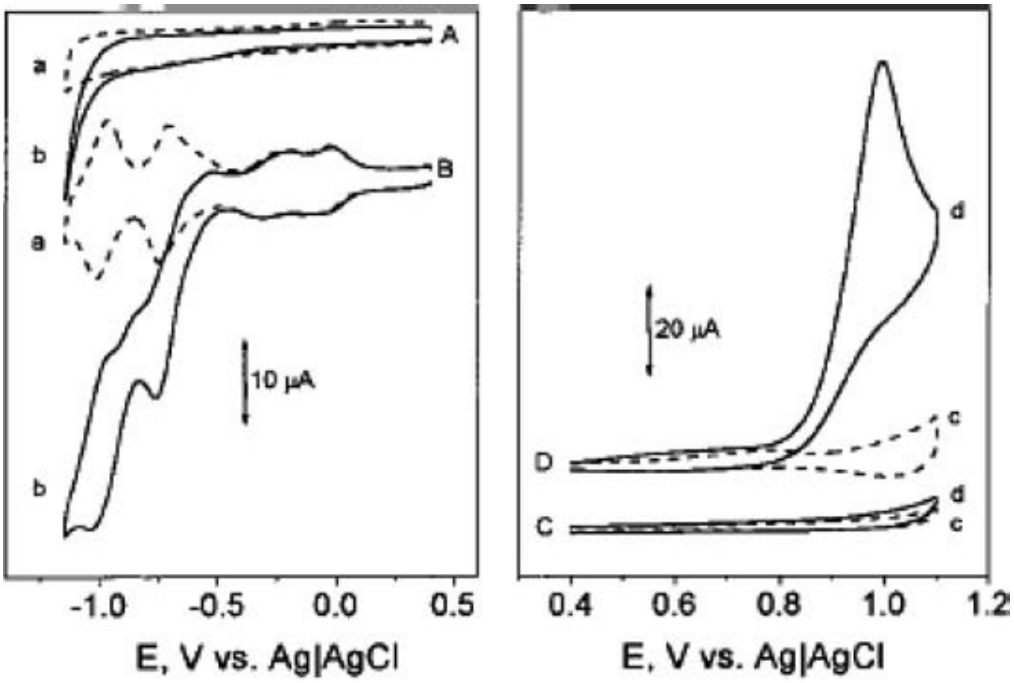

Fig. 6. Left: Reduction of iodate at a bare glassy carbon electrode (A) and a $(P_2W_{18}O_{62}^{6-}/RuDen)_{10}$-coated electrode (B). The mediated reduction of iodate by the multilayer is demonstrated by the amplification of the $P_2W_{18}O_{62}^{6-}$ reduction peak currents. **Right**: oxidation of arsenite at a bare glassy carbon electrode (C) and a $(P_2W_{18}O_{62}^{6-}/RuDen)_{10}$-coated electrode (D). The mediated oxidation of arsenite by the multilayer is demonstrated by the amplification of the reduction peak current for the oxidation of Ru^{II}. (Adapted from Ref. 26.)

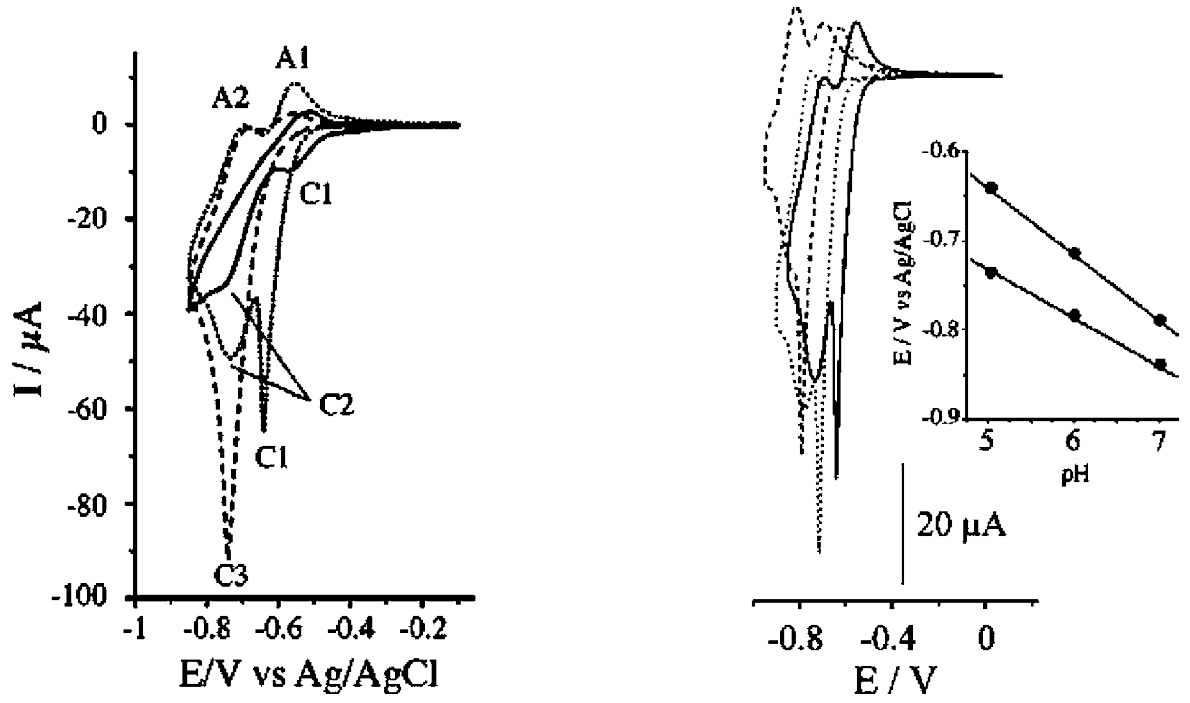

Fig. 7. **Left**: CVs of (PSS/PAH/**Co-POM**/PAH)$_{10}$ (solid) assembled with salt-free solutions, (PSS/PAH/**Co-POM**/PAH)$_{10}$ (dashed) and PSS/PAH/(**Co-POM**/PAH)$_{10}$ (dotted) assembled with PAH solution containing NaCl (0.5 M). (ITO electrode, supporting electrolyte: 0.2 M pH 5.0 PBS, scan rate: 10 mV/s.) **Right**: CVs of PSS/PAH(Co-POM/PAH)$_{10}$ assembled with PAH solution containing NaCl (0.5 M). Solid line: pH 5.0, dotted line: pH 6.0, dashed line: pH 7.0. The insert shows the dependence of redox potentials on pH (ITO electrode, supporting electrolyte: 0.2 M PBS, scan rate: 10 mV/s.) (Adapted from Ref. 22b.)

ITO electrode assembled from salt-free PAH solution (solid line) shows redox waves with peaks at −0.574 V (C1) and 0.73 V (C2) and 0.52 (A1). A different electrochemical response is observed if the film is assembled with a PAH solution containing NaCl (0.5 M). During the cathodic sweep, only one reduction peak appears at a potential of −0.744 V (C3), and during the anodic sweep two peaks appear at −0.563 (A1) and −0.687 (A2). Apparently, the two two-electron reduction steps merge into one four-electron process. Yet, a different response is observed if the layer sequence is altered. The CV of a (**Co-POM**/PAH)$_{10}$ multilayer (dotted line) assembled with PAH containing NaCl (0.5 M) exhibits two peaks at potentials of −0.643 (C1) and −0.731 (C2) during the cathodic sweep, and two peaks at −0.554 (A1) and −0.69 (A2) during anodic sweep, respectively. These examples demonstrate that the redox properties of the immobilized **Co-POM** can reveal subtle variations in film structure and composition [30]. This property suggests the use of POMs as electroactive probe to study mircoenvironmental effects in ELSA multilayers.

The voltammetric response of ELSA-based **Co-POM** multilayer is also pH-dependent. Representative CVs as a function of the pH are shown in Fig. 7. The relationship between redox potential and pH is shown in the

insert. With decreasing pH, the redox potentials shift to positive potential. This feature makes **Co-POM** based multilayers potential candidates for pH microsensors, e.g., in physiological media. Our approach has several advantages over other pH sensors [31]: it is simple and inexpensive to fabricate, operates reversibly, the layers have long-term stability and, in addition, the electrochemical response characteristics, such as sensitivity and response time, can be adjusted by the structure and composition of the sensing layer.

CONCLUSIONS

Electrostatic interactions can be employed to assemble POMs in surface confined multilayers. Formation of ELSA multilayers of POMs and oppositely charged moieties is a straightforward procedure for thin film fabrication, which offers a number of important advantages, for example, the ease of preparation, the high degree of structural and functional control, the availability of suitable charged functional and structural components, as well as the stability of the resulting layers. POM multilayers are promising candidates for diverse applications including electrocatalytic, photo- and electro-chromic systems. The results observed until now are still quite limited. Further studies are necessary to elucidate the full potential of these materials.

ABBREVIATIONS

CTA: cetyltrimethylammonium
CuPEI: solutions of copper complexes with polyethylenimine
DADD: 1,10-diaminodecane
DTA: dodecyltrimethylammonium
ITO: indium tin oxide
ELSA: electrostatic layer-by-layer self-assembly
PAH: poly(allylamine hydrochloride)
PDDA: poly(diallyldimethylammonium chloride)
PE: polyelectrolyte
PEI: poly(ethyleneimine)
POM: polyoxometalate
PSS: sodium poly(4-styrenesulfonate)
$PVPH^+$: protonated poly(4-vinylpyridine)
RuDen: pentaerythritol-based metallodendrimer with Ru^{II} terpyridine unit
SEC: surfactant-encapsulated cluster

ACKNOWLEDGMENTS

D.G.K. and D.V. thank the BMBF, DFG, and the VW foundation for financial support. D.V. thanks the DFG for a Habilitanden fellowship. Valuable discussions with Helmuth Mohwald and Achim Muller are gratefully acknowledged.

REFERENCES

1. (a) I. V. Kozhevnikov (1998). *Chem. Rev.* **98**, 171. (b) N. Mizuno and M. Misono (1998). *Chem. Rev.* **98**, 199.
2. (a) I. A. Weinstock (1998). *Chem. Rev.* **98**, 113. (b) M. Sadakane and E. Steckhan (1998). *Chem. Rev.* **98**, 219.
3. T. Yamase (1998). *Chem. Rev.* **98**, 307.
4. J. T. Rhule, C. L. Hill, D. A. Judd, and R. F. Schinazi (1998). *Chem. Rev.* **98**, 327.
5. D. E. Katsoulis (1998). *Chem. Rev.* **98**, 359.
6. J. F. Keggin (1933). *Nature* **131**, 908.
7. Intriguing examples include the "giant wheel," the Keplerate cluster, or the very recently discovered "nano-hedgehog." (a) A. Muller, E. Krickemeyer, J. Meyer, H. Bogge, F. Peters, W. Plass, E. Diemann, S. Dillinger, F. Nonnenbruch, M. Randerath, and C. Menke (1995). *Angew. Chem. Int. Ed. Engl.* **34**, 2122. (b) A. Muller, E. Krickemeyer, H. Bogge, M. Schmidtmann, and F. Peters (1998). *Angew. Chem. Int. Ed. Engl.* **37**, 3360. (c) A. Muller, E. Beckmann, H. Bogge, M. Schmidtmann, and A. Dress (2002). *Angew. Chem. Int. Ed. Engl.* **41**, 1162.
8. (a) M. T. Pope, *in* D. B. Brown (ed.), *Mixed Valence Compounds* (Reidel, Dordrecht, 1980), pp. 365. (b) M. T. Pope (1991). *Prog. Inorg. Chem.* **39**, 181.
9. M. Sadakane and E. Steckhan (1998). *Chem. Rev.* **98**, 219.
10. (a) A. Muller, S. K. Das, M. O. Talismanova, H. Bogge, P. Kogerler, M. Schmidtmann, S. S. Talismanov, M. Luban, and E. Krickemeyer (2002). *Angew. Chem. Int. Ed. Engl.* **41**, 579. (b) A. Muller, E. Krickemeyer, S. K. Das, P. Kogerler, S. Sarkar, H. Bogge, M. Schmidtmann, and S. Sarkar (2000). *Angew. Chem. Int. Ed. Engl.* **39**, 1612. (c) A. Muller, E. Diemann, C. Kuhlmann, W. Eimer, C. Serain, T. Tak, A. Knochel, and P. K. Pranzas (2001). *Chem. Commun.*, 1928. (d) T. Liu (2002). *J. Am. Chem. Soc.* **124**, 10942. (e) T. Liu, Q. Wan, Y. Xie, C. Burger, L.-Z. Liu, and B. Chu (2001). *J. Am. Chem. Soc.* **123**, 10966. (f) T. Liu (2003). *J. Am. Chem. Soc.* **125**, 312.
11. J. D. Swalen, D. L. Allara, J. D. Andrade, E. A. Chandross, S. Garoff, J. Israelachvili, T. J. McCarthy, R. Murray, R. F. Pease, J. F. Rabolt, K. J. Wynne, and H. Yu (1987). *Langmuir* **3**, 932.
12. (a) D. G. Kurth, P. Lehmann, D. Volkmer, A. Muller, and D. Schwahn (2000). *J. Chem. Soc. Dalton Trans.* **21**, 3989. (b) D. Volkmer, A. Du Chesne, D. G. Kurth, H. Schnablegger, P. Lehmann, M. J. Koop, and A. Muller (2000). *J. Am. Chem. Soc.* **122**, 1995. (c) D. G. Kurth, P. Lehmann, D. Volkmer, H. Colfen, M. J. Koop, A. Muller, and A. Du Chesne (2000). *Chem. Eur. J.* **6**, 385.
13. D. Volkmer, B. Bredenkotter, J. Tellenbroker, P. Kogerler, D. G. Kurth, P. Lehmann, H. Schnablegger, D. Schwahn, M. Piepenbrink, and B. Krebs (2002). *J. Am. Chem. Soc.* **124**, 10489.
14. G. Decher (1997). *Science* **277**, 1232.
15. D. G. Kurth and T. Bein (1995). *Langmuir* **11**, 3061.

16. (a) V. Chechik and C. J. M. Stirling, *in* S. Patai and Z. Rappoport (eds.), *The Chemistry of Organic Derivatives of Gold and Silver* (Wiley, 1999), pp. 551. (b) A. Ulman, *An Introduction to Ultrathin Organic Films: From Langmuir–Blodgett to Self-Assembly* (Academic Press, New York, 1991).
17. D. G. Kurth and R. Osterhout (1999). *Langmuir* **15**, 4842.
18. (a) D. Ingersoll, P. J. Kulesza, and L. R. Faulkner (1994). *J. Electrochem. Soc.* **141**, 140. (b) A. Kuhn and F. C. Anson (1996). *Langmuir* **12**, 5481. (c) C. Q. Sun and J. D. Zhang (1998). *Electrochim. Acta* **43**, 943. (d) L. Cheng and S. J. Dong (1999). *Electrochem. Commun.* **1**, 159.
19. (a) I. Moriguchi and J. H. Fendler (1998). *Chem. Mater.* **10**, 2205. (b) I. Ichinose, H. Tagawa, S. Mizuki, Y. Lvov, and T. Kunitake (1998). *Langmuir* **14**, 187.
20. D. G. Kurth, D. Volkmer, M. Ruttorf, B. Richter, and A. Muller (2000). *Chem. Mater.* **12**, 2829.
21. F. Caruso, D. G. Kurth, D. Volkmer, M. J. Koop, and A. Muller (1998). *Langmuir* **14**, 3462.
22. (a) S. Liu, D. G. Kurth, B. Bredenkotter, and D. Volkmer (2002). *J. Am. Soc. Chem.* **124**, 12279. (b) S. Liu, D. G. Kurth, and D. Volkmer (2002). *Chem. Commun.*, 976.
23. (a) S. Liu, D. G. Kurth, H. Mohwald, and D. Volkmer (2002). *Adv. Mater.* **14**, 225. (b) L. Xu, H. Y. Zhang, E. Wang, D. G. Kurth, and Z. Li (2002). *J. Mater. Chem.* **12**, 654.
24. (a) A. Kuhn, N. Mano, and C. Vidal (1999). *J. Electroanal. Chem.* **462**, 187. (b) Z. H. Chen, Y. Ma, X. T. Zhang, B. Liu, and J. N. Yao (2001). *J. Coll. Inter. Sci.* **240**, 487.
25. L. Cheng and J. A. Cox (2002). *Chem. Mater.* **14**, 6.
26. M. Losche, J. Schmitt, G. Decher, W. G. Bouwman, and K. Kjaer (1998). *Macromolecules* **31**, 8893.
27. J. Schmitt, T. Grunewald, G. Decher, P. S. Pershan, K. Kjaer, and M. Losche (1993). *Macromolecules* **26**, 7058.
28. M. Tarabia, H. Hong, D. Davidov, S. Kirstein, R. Steitz, R. Neumann, and Y. Avny (1998). *J. Appl. Phys.* **83**, 725.
29. M. R. Antonio and L. Soderholm (1997). *J. Alloys Compounds* **250**, 541.
30. A. Mahmoud, B. Keita, L. Nadjo, O. Oung, R. Contant, S. Brown, and Y. de Kouchkovsky (1999). *J. Electroanal. Chem.* **463**, 129.
31. J. Lin (2000). *Trends Anal. Chem.* **19**, 541.